separations

MDPI

*Article*

# Characterization of the Binding Behavior of Specific Cobalt and Nickel Ion-Binding Peptides Identified by Phage Surface Display

**Sabine Matys *, Lisa-Marie Morawietz, Franziska Lederer and Katrin Pollmann**

Helmholtz-Zentrum Dresden-Rossendorf, Helmholtz Institute Freiberg for Resource Technology, Bautzner Landstraße 400, 01328 Dresden, Germany
* Correspondence: s.matys@hzdr.de

**Abstract:** In recent years, the application focus of phage surface display (PSD) technology has been extended to the identification of metal ion-selective peptides. In previous studies, two phage clones—a nickel-binding one with the peptide motif CNAKHHPRCGGG and a cobalt-binding one with the peptide motif CTQMLGQLCGGG—were isolated, and their binding ability to metal-loaded NTA agarose beads was investigated. Here, the free cyclic peptides are characterized by UV/VIS spectroscopy with respect to their binding capacity for the respective target ion and in crossover experiments for the other ion by isothermal titration calorimetry (ITC) in different buffer systems. This revealed differences in selectivity and affinity. The cobalt-specific peptide is very sensitive to different buffers; it has a 20-fold higher affinity for cobalt and nickel under suitable conditions. The nickel-specific peptide binds more moderately and robustly in different buffers but only selectively to nickel.

**Keywords:** phage surface display; biopanning; metal-binding peptides; nickel; cobalt; isothermal titration calorimetry

check for updates

**Citation:** Matys, S.; Morawietz, L.-M.; Lederer, F.; Pollmann, K. Characterization of the Binding Behavior of Specific Cobalt and Nickel Ion-Binding Peptides Identified by Phage Surface Display. *Separations* **2022**, *9*, 354. https://doi.org/10.3390/separations9110354

Academic Editor: Marco Brucale

Received: 30 September 2022
Accepted: 1 November 2022
Published: 7 November 2022

**Publisher's Note:** MDPI stays neutral with regard to jurisdictional claims in published maps and institutional affiliations.

**Copyright:** © 2022 by the authors. Licensee MDPI, Basel, Switzerland. This article is an open access article distributed under the terms and conditions of the Creative Commons Attribution (CC BY) license (https://creativecommons.org/licenses/by/4.0/).

## 1. Introduction

The fundamental understanding and utilization of natural material cycles and operation principles will open up completely new possibilities for the current economic challenges and deliver perspectives for a future-oriented and sustainable circular economy [1–3]. Naturally occurring processes are often characterized by special effectiveness, specificity and selectivity. These special properties are exhibited by proteins and peptides, which are macromolecules modulated by evolution. Therefore, they are also the subject of diverse research when it comes to developing new, innovative and more cost-effective biotechnological processes and materials with high efficiency. Peptides, in particular, are highly attractive as new adaptable bioreagents in many different applications. Currently, unattractive industrial wastewaters with low metal concentrations are attractive case studies for the development of bio-based metal recycling strategies. In addition to the screening of naturally occurring molecules, genetic engineering methods are being exploited today under the concept of directed evolution [4–6]. For the identification of these peptides, we used the so-called phage surface display (PSD) technology. Bacteria-infecting viruses, so-called bacteriophages, play an exposed role in this process, as their simple structure makes them easily accessible to genetic modifications [7,8]. Moreover, they can be easily amplified and purified in large numbers [9]. The direct link between genotype and phenotype makes it easy to express additional peptide sequences on the viral surface. In this way, for example, randomized libraries with a tremendous number of diverse peptide motifs can be generated and screened against almost any target [10–12]. Since its introduction to the scientific world in 1985 by George P. Smith, the PSD technique has become an almost universal tool for a constantly growing number of different questions and applications [10,13]. To date, more than 33,000 peptide sequences have been deposited in the Biopanning Data Bank [14].

In the first decades, the main focus was on the search for specific binding peptides for medical and pharmaceutical applications, such as antibody development [15], epitope mapping [16,17], drug discovery [18–20], investigation of protein-protein interactions [21–23], and nanotechnological applications [24–27]. New fields of application are increasingly emerging, such as the search for binding peptides for inorganic surfaces [28–30], sensor development [31–34], or the removal of toxic or economically significant metal ions from complexly composed aqueous streams [35–38]. We developed highly selective peptide-based materials for resource recovery applications. PSD is used to identify the specific binding peptide sequences. With its help, suitable selective binding structures can be found for virtually any chemical element. For example, in a previous study, nickel- and cobalt-binding phage clones from the Ph.D.™-C7C Phage Display Peptide Library (New England Biolabs GmbH, Frankfurt/Main, Germany) were identified and their binding properties to NTA agarose beads were described [37,39]. The nickel-binding phage clone with the motif CNAKHHPRCGGG and the cobalt-binding clone with the motif CTQMLGQLCGGG were identified as the best binders. Since the use of complete phages for real applications is impractical for various reasons, testing the binding properties of the isolated peptides is an indispensable further step on the path of material development. Therefore, in this study, the two cyclic peptides with a disulfide bridge between the cysteine residues were commercially synthesized, and their metal-binding properties were investigated using UV/VIS spectroscopy and isothermal titration calorimetry (ITC).

## 2. Materials and Methods

### *2.1. Chemicals and Buffers*

All chemicals used were of analytical grade. $NiCl_2 \times 6H_2O$ was from Merck Chemicals GmbH, Germany, and $CoCl_2 \times 6H_2O$ was purchased from Sigma Aldrich. An amount of 0.01 M of N-(2-hydroxyethyl)-piperazine-N′-(2-ethanesulfonic acid)-buffer (HEPES, Carl Roth GmbH, Karlsruhe, Germany) with 0.03 M NaCl, and 0.05 M 3-(N-morpholino)propanesulfonic acid (MOPS, Carl Roth GmbH, Karlsruhe, Germany) with 0.15 M NaCl, and 0.01 M and 0.05 M Tris-Buffered Saline (Tris-HCl, Carl Roth GmbH, Karlsruhe, Germany) with 0.03 and 0.15 M NaCl, respectively, was prepared with MilliQ water and degassed by autoclaving. Cyclic peptides with a disulfide bridge between the cysteine residues were purchased as TFA salts with >95% purity from GL Biochem Ltd., Shanghai, prepared as 0.02 M stock solutions in MilliQ water, and stored in aliquots at −20 °C until use. The cyclic structure of the two peptides was confirmed by LC-ESI-MS (SI, Figures S14 and S15).

### *2.2. UV/VIS Spectroscopy*

A Silver Nova Stellarnet spectrometer was used for UV/VIS measurements of the Ni- and Co-peptide complexes (Scientific Instruments GmbH, Gilching, Germany). All peptide and metal salt solutions at different concentrations were prepared in 11.69 g/L NaCl, and had a pH of 7.4. Metal salt and peptide solutions of different mole fractions were mixed, and the absorption spectra were recorded. The stoichiometry of the complexes was estimated using the continuous variations method or the Job method. For this purpose, the absorbance values of the characteristic electron transition peaks were plotted against the mol fraction.

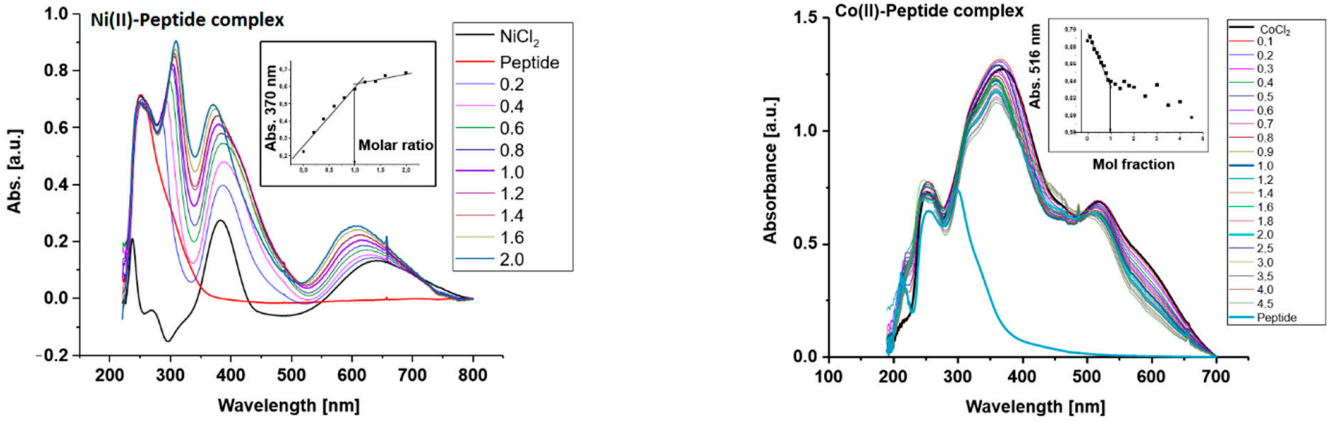
### *2.3. Isothermal Titration Calorimetry*

We used a MicroCal PEAC-ITC (Malvern Panalytical GmbH, Kassel, Germany) for our experiments using a standard protocol. The measuring cell contained 280 µL buffer with 0.2–0.4 mM peptide. The syringe was filled with 2–4 mM $NiCl_2$ or $CoCl_2$ solution in the same buffer. The injections were performed in 19 single steps of 2 µL each, except for the first injection of 0.4 µL with an injection time of 4 s and an interval of 150 s each. The reference power was 10 µcal/s. The stirring speed was 750 rpm. The control software MicroCal PEAQ-ITC, version 1.40, was used for instrument control and MicroCal PEAQ-ITC, version 1.41, for data evaluation. If saturation of the bond was not yet reached after

the first titration run, an additional metal salt solution was titrated in a subsequent run. The raw data for these two measurements were merged using the Malvern Panalytical software tool MicroCal Concat, version 1.0. The heat of dilution generated when titrating the metal salt solutions into the measuring cell was determined by control measurements with a metal salt solution to buffer and subtracted from the measured data of complex formation. On the other hand, the influences of the titrations from buffer to buffer and from buffer to peptide solution are generally much smaller and, therefore, negligible [40].

## 3. Results

The UV/VIS spectra of the solutions containing cobalt and nickel showed characteristic electron transition peaks, which can be used to determine the stoichiometry of the formed complexes with both cyclic peptides. The absorbance values plotted against the mole fractions at 370 and 516 nm for nickel- and cobalt-containing solutions, respectively, showed a kink in the straight line in each case at a molar ratio of 1, indicating a stoichiometry of 1:1 for both complexes (see Figure 1).




(**a**) (**b**)

**Figure 1.** UV/VIS absorption spectra and Job plots of different molar ratios of (**a**) the cyclic nickel-binding peptide CNAKHHPRCGGG with $Ni^{2+}$ ions and (**b**) the cyclic cobalt-binding peptide CTQML-GQLCGGG with $Co^{2+}$ ions. All reactants were dissolved in 11.69 g/L NaCl, pH 7.4.

The isothermal titration experiments revealed different thermodynamic parameters for the two cyclic peptides and, as expected, differences in binding behavior in different buffers (Table 1). The data of most titration experiments were best fit with a one-site binding model (see also supplementary information).

The cyclic nickel-binding peptide with the motif CNAKHHPRCGGG showed complexation with $Ni^{2+}$ ions in TBS, MOPS, and HEPES buffers, all containing NaCl, and had a pH of 7.4. Figure 2a shows an example of a measurement taken from a TBS buffer. The complexation process required a double titration to achieve saturation of the reaction. As can be seen from the legend, the N value is just below 1, which corresponds to a stoichiometry of 1:1. These findings support the results from UV/VIS measurements. For the complexation in MOPS buffer with the same ionic background of NaCl (Figure 2b), the N value is well below 0.5, which corresponds to a stoichiometry of two cyclic peptide molecules to one metal ion. Interestingly, the values for the change in free energy are approximately the same, while the values for the change in enthalpy are significantly different in MOPS. The values for $-T\Delta S$ are also relatively far apart. The affinity constants are nearly identical. The values obtained in HEPES and NaCl with a concentration of a factor of five or lower are very similar to those for the binding in MOPS buffer (Table 1). No binding was detected for lower-concentrated TBS with NaCl.

**Table 1.** Thermodynamic parameters of complex formation of $Ni^{2+}$ specific binding cyclic peptide CNAKHHPRCGGG and $Co^{2+}$-binding cyclic peptide CTQMLGQLCGGG with the respective metal ion and vice versa. All buffers had a pH of 7.4.

| Peptide | Conc. (g/L) | Metal Ion | Conc. (g/L) | Buffer (g/L) | N | $K_D$ (M) | ΔH (kJ/mol) | ΔG (kJ/mol) | −TΔS (kJ/mol) |
|---|---|---|---|---|---|---|---|---|---|
| CNAKHHPRCGGG | 0.284 | $Ni^{2+}$ | 0.2113 | 6.057 Tris-HCl 8.766 NaCl | $0.822 \pm 5.9 \times 10^{-2}$ | $1.04 \times 10^{-4} \pm 1.38 \times 10^{-5}$ | $-18.7 \pm 1.70$ | −22.8 | −4.03 |
| | 0.495 | $Ni^{2+}$ | 0.2348 | 10.463 MOPS 8.766 NaCl | $0.397 \pm 2.4 \times 10^{-2}$ | $1.87 \times 10^{-4} \pm 2.27 \times 10^{-5}$ | $-36.4 \pm 4.14$ | −21.3 | 15.1 |
| | 0.495 | $Ni^{2+}$ | 0.2348 | 2.383 HEPES 1.753 NaCl | $0.564 \pm 3.1 \times 10^{-2}$ | $2.88 \times 10^{-4} \pm 1.76 \times 10^{-5}$ | $-26.3 \pm 1.86$ | −20.2 | 6.08 |
| | 0.495 | $Ni^{2+}$ | 0.2348 | 1.211 Tris-HCl 1.753 NaCl | 0 | 0 | 0 | 0 | 0 |
| CNAKHHPRCGGG | 0.284 | $Co^{2+}$ | 0.0589 | 6.057 Tris-HCl 8.766 NaCl | 0 | 0 | 0 | 0 | 0 |
| CTQMLGQLCGGG | 0.552 | $Co^{2+}$ | 0.0589 | 1.211 Tris-HCl 1.753 NaCl | $1.04 \pm 7.8 \times 10^{-3}$ | $5.09 \times 10^{-6} \pm 6.03 \times 10^{-7}$ | $-35.6 \pm 0.342$ | −30.2 | 5.35 |
| | 0.502 | $Co^{2+}$ | 0.236 | 6.057 Tris-HCl 8.766 NaCl | 0 | 0 | 0 | 0 | 0 |
| | 0.502 | $Co^{2+}$ | 0.236 | 10.463 MOPS 8.766 NaCl | 0 | 0 | 0 | 0 | 0 |
| | 0.502 | $Co^{2+}$ | 0.236 | 2.383 HEPES 1.753 NaCl | 0 | 0 | 0 | 0 | 0 |
| CTQMLGQLCGGG | 0.2760 | $Ni^{2+}$ | 0.0587 | 1.211 Tris-HCl 1.753 NaCl | $0.837 \pm 7.8 \times 10^{-3}$ | $7.69 \times 10^{-6} \pm 6.59 \times 10^{-7}$ | $-35.6 \pm 0.434$ | −29.2 | 6.40 |

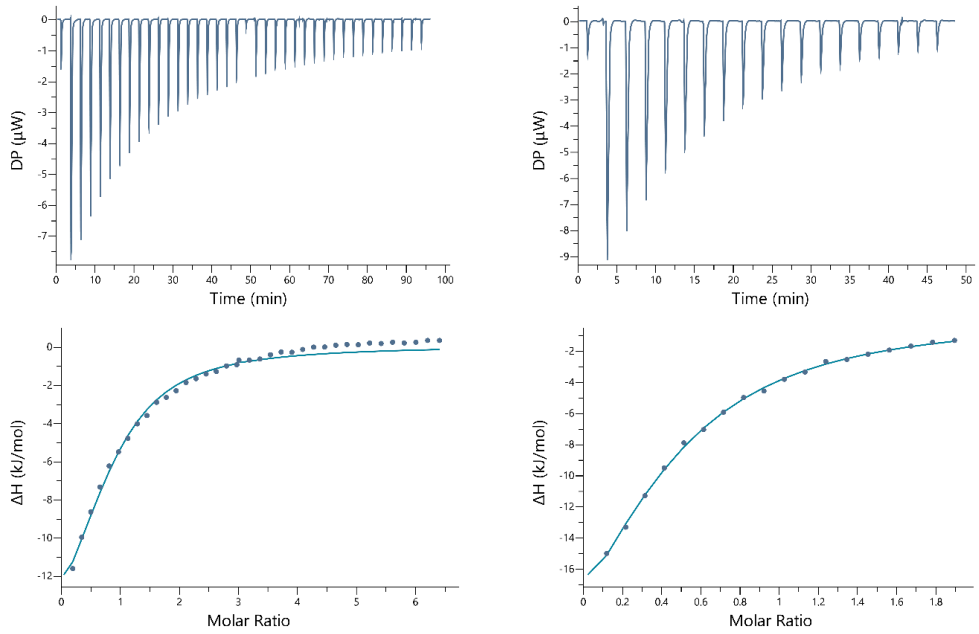



**Figure 2.** Isothermal titration calorimetry results of the cyclic nickel-binding peptide CNAKHHPRCGGG with $Ni^{2+}$ ions. Top: raw heat rate (µW) vs. time (min). Bottom: changes in enthalpy (kJ/mol) vs. molar ratio of the reactants. (**a**) Tris-HCl + NaCl, pH 7.4; (**b**) MOPS + NaCl, pH 7.4. The data were fitted using a one-set-of-sites model.

In contrast, the cobalt-binding cyclic peptide with the motif CTQMLGQLCGGG showed a different performance. Neither in HEPES with NaCl, nor in MOPS with NaCl, nor higher concentrated TBS with NaCl complexation with $Co^{2+}$ occurred. Only in a TBS with NaCl concentrated five times lower could a complexation be detected. Figure 3 shows that the curve followed an almost ideal sigmoidal Wiseman plot. The stoichiometry of the complex formed is 1:1. The entropic contribution is relatively small. The enthalpy change, on the other hand, represents a considerable contribution to the complexation reaction. With an affinity constant of $5.09 \times 10^{-6}$ M $\pm$ $6.03 \times 10^{-7}$, this peptide has a 20-fold greater affinity for its target ion compared with the nickel-binding cyclic peptide.

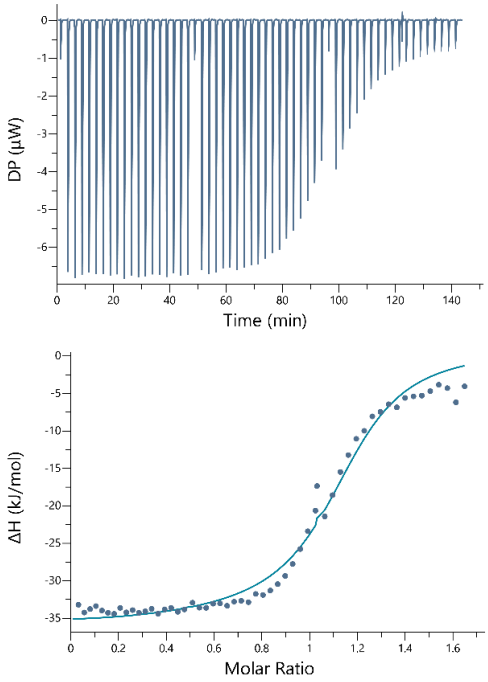
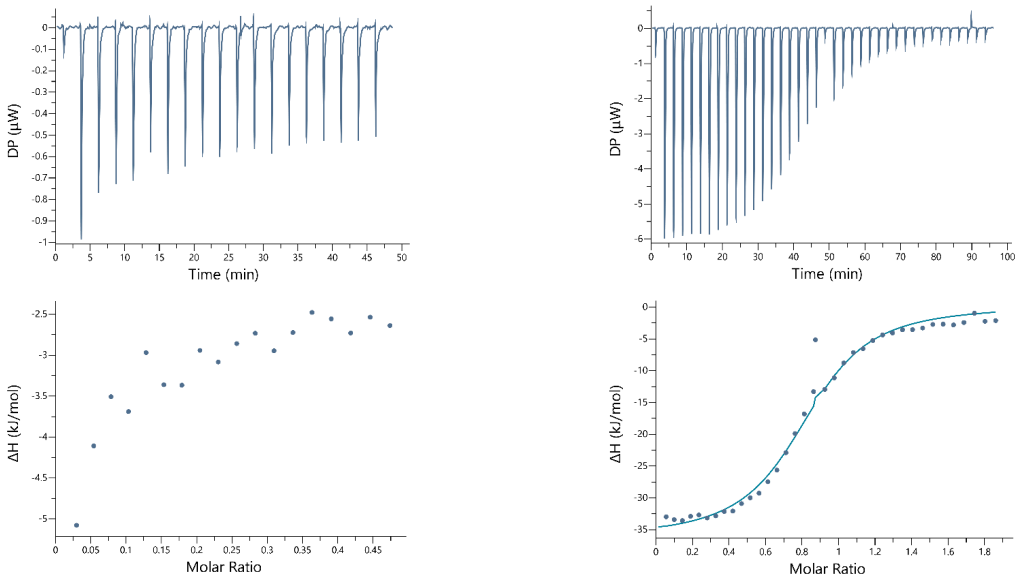



**Figure 3.** Isothermal titration calorimetry results of the cyclic cobalt-binding peptide CTQMLGQL-CGGG with $Co^{2+}$ ions in Tris-HCl + NaCl, pH 7.4. Top: raw heat rate (µW) vs. time (min). Bottom: changes in enthalpy (kJ/mol) vs. molar ratio of the reactants. The data were fitted using a one-set-of-sites model.

Additional cross-binding experiments were performed with both cyclic peptides to demonstrate selectivity (Figure 4). The cobalt-binding peptide was found to interact with $Ni^{2+}$ as well, with a nearly identical affinity of $K_D = 7.69 \times 10^{-6}$ M $\pm$ $6.59 \times 10^{-7}$ and similar enthalpic and entropic contributions. In contrast, no interaction was detectable between the nickel-binding peptide and $Co^{2+}$.




(**a**) (**b**)

**Figure 4.** Isothermal titration calorimetry results of the cyclic nickel-binding peptide CNAKHHPRCGGG with $Co^{2+}$ ions in TBS + NaCl, pH 7.4 (**a**) and the cyclic cobalt-binding peptide CTQMLGQLCGGG with $Ni^{2+}$ ions in TBS + NaCl, pH 7.4 (**b**). Top: raw heat rate (µW) vs. time (min). Bottom: changes in enthalpy (kJ/mol) vs. molar ratio of the reactants. The data were fitted using a one-set-of-sites model.

## 4. Discussion

The aim of our work was to characterize the earlier identified peptides that can distinguish between the chemically very similar elements cobalt and nickel, thus making it possible to separate both elements selectively from each other from aqueous mixtures.

For the characterization of the synthesized cyclic peptides, the complex formation with the respective metal salt was investigated with UV/VIS spectroscopy and isothermal titration calorimetry. Thanks to the absorption behavior of cobalt and nickel ions in the visible range, the stoichiometry of the complexes formed can be determined using the continuous variation method. For complexes of both peptides with the respective target ion, specifically, a nickel-binding peptide with nickel and a cobalt-binding peptide with cobalt, a stoichiometry of 1:1 was found. However, this method has some limitations in such cases when more than one complex species is formed between the metal ion and the peptide, but these cannot be discussed in detail here [41–43]. One of the disadvantages is the relatively large amount of peptide required for spectroscopic measurements, which is a limiting factor. The use of highly sensitive microcalorimetry represents a convincing alternative in this respect. The titration experiments with ITC clearly showed that there are differences in binding behavior between both cyclic nickel- and cobalt-binding peptides. The cross-measurements showed that although the nickel peptide is a rather moderate binder overall, it selectively binds to nickel in TBS with NaCl at higher ionic strength. No interaction with cobalt could be detected under these conditions. The cobalt-binding peptide, in turn, was not selective in TBS buffer containing NaCl with fivefold reduced ionic strength. The pI values for both peptides themselves provide evidence for differences in binding behavior. The nickel peptide has a value of 11.48, so it is positively charged at a pH of 7.4. The cobalt peptide, on the other hand, with a pI value of 3.97, is negatively charged in the neutral range. This could give an indication of the lack of selectivity. The different behavior of both peptides in different buffer systems was also remarkable. While the nickel-binding peptide was active with a high ionic background, the cobalt-binding peptide was very sensitive in these environments. Comparing the performance of the nickel-binding peptide in TBS and MOPS buffers with a higher ionic background of NaCl, it is noticeable that the free or Gibbs energy contributions are almost identical, while the enthalpic and entropic fractions significantly differ. This often observed and still discussed phenomenon is described as enthalpy-entropy compensation (EEC) [44–46]. This behavior of the reactants describes physical changes emanating from the reorganization/release of water, change of hydrogen bonds, and change of peptide conformation and hydrophobic interactions. It can be further assumed that the functional side chains of cysteine, methionine, histidine as well as glutamic acid, tyrosine and others are mainly responsible for the interaction between a metal ion and peptide [47]. Some are present in both the nickel-binding peptide CNAKHHPRCGGG and the cobalt-binding peptide CTQMLGQLCGGG. Possible metal-binding sites in these peptides have already been discussed in detail by Braun et al. [37]. The negative free energy contributions in all measured complexation reactions indicate spontaneously occurring reactions. In all these reactions, enthalpic contributions were significantly larger than entropic ones, suggesting a stronger involvement of solvation processes. The lower entropic contributions suggest that hydrophobic interactions or conformational changes play a minor role. ITC has proven to be a very well-suited tool for the sensitive measurement of the interaction of peptides with metal ions. However, when interpreting the data, it must be taken into account that very complex processes are involved, in which thermal contributions are made, for example, by protonation processes, dilution reactions or complex formations between metal ions and buffer. A careful data interpretation must also take into account possible sources of error, such as pH changes, changes in ion concentration, denatured portions of the peptide, etc. In the meantime, there are a large number of publications that address these processes and provide possible solutions [48–52]. However, with due caution, the data obtained using ITC provides valuable information for the characterization and screening of metal ion-binding peptides.

In addition, modern, highly sensitive measuring microcalorimeters offer a high degree of time and cost savings thanks to the small volume of material required.

## 5. Conclusions

Using the two chemically similar elements nickel and cobalt as an example, we have shown how UV/VIS spectroscopy and isothermal titration calorimetry (ITC) can be used to characterize stoichiometry, binding strength and selectivity of one nickel-binding peptide CNAKHHPRCGGG and one cobalt-binding peptide CTQMLGQLCGGG. While the cobalt-binding peptide showed better affinities of about factor 20 for both elements, the more moderately binding nickel peptide showed selectivity for its target ion under these particular experimental conditions. Using the highly sensitive ITC technique, various thermodynamic parameters of the molecular binding events between metal ions and peptides could be reliably and reproducibly detected. ITC has now become an indispensable tool for the characterization of peptides.

**Supplementary Materials:** The following supporting information can be downloaded at: https://www.mdpi.com/article/10.3390/separations9110354/s1.

**Author Contributions:** Conceptualization, K.P. and F.L.; methodology, S.M. and L.-M.M.; validation, S.M., K.P. and F.L.; investigation, S.M. and L.-M.M.; resources, S.M.; data curation, S.M. and L.-M.M.; writing—original draft preparation, S.M.; writing—review and editing, K.P. and F.L.; visualization, S.M. and L.-M.M.; supervision, S.M., K.P. and F.L.; project administration, K.P. and F.L.; funding acquisition, K.P. and F.L. All authors have read and agreed to the published version of the manuscript.

**Funding:** This research was funded by the German Ministry of Education and Research (BMBF) in the French-German Project "EcoMetals," grant number 033RF001A and the Indo-German (IGSTC) Project "BioCuInGe", grant number 01DQ17021A.

**Data Availability Statement:** Any necessary data can be provided upon request.

**Acknowledgments:** We thank Björn Drobot for helpful discussions regarding the interpretation of the ITC data and Falk Lehmann for the LC-MS measurements.

**Conflicts of Interest:** The authors declare no conflict of interest. The funders had no role in the design of the study; in the collection, analyses, or interpretation of data; in the writing of the manuscript; or in the decision to publish the results.

## References

1. Gislev, M.; Grohol, M. *Report on Critical Raw Materials and the Circular Economy*; Directorate-General for Internal Market, Industry, Entrepreneurship and SMEs, EU Commission: Brussels, Belgium, 2018.
2. Graf, P. *Die Werkzeuge der Bioökonomie*; BMBF: Berlin, Germany, 2021.
3. BMBF. *Bioökonomie Als Gesellschaftlicher Wandel*; BMBF: Berlin, Germany, 2021.
4. Packer, M.S.; Liu, D.R. Methods for the directed evolution of proteins. *Nat. Rev. Genet.* **2015**, *16*, 379–394. [CrossRef] [PubMed]
5. Cobb, R.E.; Chao, R.; Zhao, H. Directed Evolution: Past, Present and Future. *AIChE J.* **2013**, *59*, 1432–1440. [CrossRef] [PubMed]
6. Bozovičar, K.; Bratkovič, T. Evolving a Peptide: Library Platforms and Diversification Strategies. *Int. J. Mol. Sci.* **2019**, *21*, 215. [CrossRef]
7. Wang, Y.; Xue, P.; Cao, M.; Yu, T.; Lane, S.T.; Zhao, H. Directed Evolution: Methodologies and Applications. *Chem. Rev.* **2021**, *121*, 12384–12444. [CrossRef]
8. Schmidt-Dannert, C. Directed Evolution of Single Proteins, Metabolic Pathways, and Viruses. *Biochemistry* **2001**, *40*, 13125–13136. [CrossRef] [PubMed]
9. DeBenedictis, E.A.; Chory, E.J.; Gretton, D.W.; Wang, B.; Golas, S.; Esvelt, K.M. Systematic molecular evolution enables robust biomolecule discovery. *Nat. Methods* **2022**, *19*, 55–64. [CrossRef] [PubMed]
10. Smith, G.P. Filamentous fusion phage: Novel expression vectors that display cloned antigens on the virion surface. *Science* **1985**, *228*, 1315–1317. [CrossRef] [PubMed]
11. Smith, G.P.; Petrenko, V.A. Phage Display. *Chem. Rev.* **1997**, *97*, 391–410. [CrossRef]
12. Arap, M.A. Phage display technology: Applications and innovations. *Genet. Mol. Biol.* **2005**, *28*, 1–9. [CrossRef]
13. Jaroszewicz, W.; Morcinek-Orłowska, J.; Pierzynowska, K.; Gaffke, L.; Węgrzyn, G. Phage display and other peptide display technologies. *FEMS Microbiol. Rev.* **2022**, *46*, fuab052. [CrossRef]
14. He, B.; Jiang, L.; Duan, Y.; Chai, G.; Fang, Y.; Kang, J.; Yu, M.; Li, N.; Tang, Z.; Yao, P.; et al. Biopanning data bank 2018: Hugging next generation phage display. *Database* **2018**, *2018*, bay032. [CrossRef] [PubMed]

15. Azzazy, H.M.E.; Highsmith, W.E. Phage display technology: Clinical applications and recent innovations. *Clin. Biochem.* **2002**, *35*, 425–445. [CrossRef]
16. Fack, F.; Hügle-Dörr, B.; Song, D.; Queitsch, I.; Petersen, G.; Bautz, E.K.F. Epitope mapping by phage display: Random versus gene-fragment libraries. *J. Immunol. Methods* **1997**, *206*, 43–52. [CrossRef]
17. Moreira, G.M.S.G.; Fühner, V.; Hust, M. Epitope Mapping by Phage Display. In *Phage Display: Methods and Protocols*; Hust, M., Lim, T.S., Eds.; Springer: New York, NY, USA, 2018; pp. 497–518.
18. Nemudraya, A.A.; Richter, V.A.; Kuligina, E.V. Phage Peptide Libraries As a Source of Targeted Ligands. *Acta Naturae* **2016**, *8*, 48–57. [CrossRef]
19. Qi, H.; Ma, M.; Lai, D.; Tao, S.-C. Phage display: An ideal platform for coupling protein to nucleic acid. *Acta Biochim. Biophys. Sin.* **2021**, *53*, 389–399. [CrossRef] [PubMed]
20. Nagano, K.; Tsutsumi, Y. Phage Display Technology as a Powerful Platform for Antibody Drug Discovery. *Viruses* **2021**, *13*, 178. [CrossRef]
21. Sidhu, S.S.; Fairbrother, W.J.; Deshayes, K. Exploring protein-protein interactions with phage display. *Chembiochem* **2003**, *4*, 14–25. [CrossRef] [PubMed]
22. Sundell, G.N.; Ivarsson, Y. Interaction analysis through proteomic phage display. *Biomed. Res. Int.* **2014**, *2014*, 176172. [CrossRef]
23. Huang, W.; Soeung, V.; Boragine, D.M.; Palzkill, T. Mapping Protein–Protein Interaction Interface Peptides with Jun-Fos Assisted Phage Display and Deep Sequencing. *ACS Synth. Biol.* **2020**, *9*, 1882–1896. [CrossRef]
24. Rakonjac, J.; Bennett, N.J.; Spagnuolo, J.; Gagic, D.; Russel, M. Filamentous bacteriophage: Biology, phage display and nanotechnology applications. *Curr. Issues Mol. Biol.* **2011**, *13*, 51–76.
25. Seker, U.O.S.; Demir, H.V. Material Binding Peptides for Nanotechnology. *Molecules* **2011**, *16*, 1426–1451. [CrossRef] [PubMed]
26. Paczesny, J.; Bielec, K. Application of Bacteriophages in Nanotechnology. *Nanomaterials* **2020**, *10*, 1944. [CrossRef] [PubMed]
27. Hyman, P.; Denyes, J. Bacteriophages in Nanotechnology: History and Future. In *Bacteriophages: Biology, Technology, Therapy*; Harper, D.R., Abedon, S.T., Burrowes, B.H., McConville, M.L., Eds.; Springer International Publishing: Cham, Switzerland, 2021; pp. 657–687.
28. Vreuls, C.; Zocchi, G.; Genin, A.; Archambeau, C.; Martial, J.; Van de Weerdt, C. Inorganic-binding peptides as tools for surface quality control. *J. Inorg. Biochem.* **2010**, *104*, 1013–1021. [CrossRef] [PubMed]
29. Kriplani, U.; Kay, B.K. Selecting peptides for use in nanoscale materials using phage-displayed combinatorial peptide libraries. *Curr. Opin. Biotechnol.* **2005**, *16*, 470–475. [CrossRef] [PubMed]
30. Sawada, T. Filamentous virus-based soft materials based on controlled assembly through liquid crystalline formation. *Polym. J.* **2017**, *49*, 639–647. [CrossRef]
31. Machera, S.J.; Niedziółka-Jönsson, J.; Szot-Karpińska, K. Phage-Based Sensors in Medicine: A Review. *Chemosensors* **2020**, *8*, 61. [CrossRef]
32. Peltomaa, R.; Benito-Peña, E.; Barderas, R.; Moreno-Bondi, M.C. Phage Display in the Quest for New Selective Recognition Elements for Biosensors. *ACS Omega* **2019**, *4*, 11569–11580. [CrossRef]
33. Wu, J.; Park, J.P.; Dooley, K.; Cropek, D.M.; West, A.C.; Banta, S. Rapid Development of New Protein Biosensors Utilizing Peptides Obtained via Phage Display. *PLoS ONE* **2011**, *6*, e24948. [CrossRef]
34. Tan, Y.; Tian, T.; Liu, W.; Zhu, Z.; Yang, C. Advance in phage display technology for bioanalysis. *Biotechnol. J.* **2016**, *11*, 732–745. [CrossRef]
35. Nian, R.; Kim, D.S.; Nguyen, T.; Tan, L.; Kim, C.-W.; Yoo, I.-K.; Choe, W.-S. Chromatographic biopanning for the selection of peptides with high specificity to $Pb^{2+}$ from phage displayed peptide library. *J. Chromatogr. A* **2010**, *1217*, 5940–5949. [CrossRef]
36. Schönberger, N.; Braun, R.; Matys, S.; Lederer, F.L.; Lehmann, F.; Flemming, K.; Pollmann, K. Chromatopanning for the identification of gallium binding peptides. *J. Chromatogr. A* **2019**, *1600*, 158–166. [CrossRef]
37. Braun, R.; Bachmann, S.; Schönberger, N.; Matys, S.; Lederer, F.; Pollmann, K. Peptides as biosorbents—Promising tools for resource recovery. *Res. Microbiol.* **2018**, *169*, 649–658. [CrossRef] [PubMed]
38. Li, H.; Dong, W.; Liu, Y.; Zhang, H.; Wang, G. Enhanced Biosorption of Nickel Ions on Immobilized Surface-Engineered Yeast Using Nickel-Binding Peptides. *Front. Microbiol.* **2019**, *10*, 1254. [CrossRef] [PubMed]
39. Matys, S.; Schönberger, N.; Lederer, F.L.; Pollmann, K. Characterization of specifically metal-binding phage clones for selective recovery of cobalt and nickel. *J. Environ. Chem. Eng.* **2020**, *8*, 103606. [CrossRef]
40. Ghai, R.; Falconer, R.J.; Collins, B.M. Applications of isothermal titration calorimetry in pure and applied research—Survey of the literature from 2010. *J. Mol. Recognit.* **2011**, *25*, 32–52. [CrossRef] [PubMed]
41. Brynn Hibbert, D.; Thordarson, P. The death of the Job plot, transparency, open science and online tools, uncertainty estimation methods and other developments in supramolecular chemistry data analysis. *ChemComm* **2016**, *52*, 12792–12805. [CrossRef]
42. Olson, E.J.; Bühlmann, P. Getting More out of a Job Plot: Determination of Reactant to Product Stoichiometry in Cases of Displacement Reactions and n:n Complex Formation. *J. Org. Chem.* **2011**, *76*, 8406–8412. [CrossRef]
43. Renny, J.S.; Tomasevich, L.L.; Tallmadge, E.H.; Collum, D.B. Method of continuous variations: Applications of job plots to the study of molecular associations in organometallic chemistry. *Angew. Chem. Int. Ed.* **2013**, *52*, 11998–12013. [CrossRef]
44. Dragan, A.I.; Read, C.M.; Crane-Robinson, C. Enthalpy–entropy compensation: The role of solvation. *Eur. Biophys. J.* **2017**, *46*, 301–308. [CrossRef]
45. Starikov, E.B.; Nordén, B. Enthalpy−Entropy Compensation: A Phantom or Something Useful? *J. Phys. Chem. B* **2007**, *111*, 14431–14435. [CrossRef]

46. Ryde, U. A fundamental view of enthalpy–entropy compensation. *MedChemComm* **2014**, *5*, 1324–1336. [CrossRef]
47. Bou-Abdallah, F.; Giffune, T.R. The thermodynamics of protein interactions with essential first row transition metals. *Biochim. Biophys. Acta* **2016**, *1860*, 879–891. [CrossRef]
48. Johnson, R.A.; Manley, O.M.; Spuches, A.M.; Grossoehme, N.E. Dissecting ITC data of metal ions binding to ligands and proteins. *Biochim. Biophys. Acta* **2016**, *1860*, 892–901. [CrossRef]
49. Grossoehme, N.E.; Spuches, A.M.; Wilcox, D.E. Application of isothermal titration calorimetry in bioinorganic chemistry. *J. Biol. Inorg. Chem.* **2010**, *15*, 1183–1191. [CrossRef] [PubMed]
50. Wyrzykowski, D.; Pilarski, B.; Jacewicz, D.; Chmurzyński, L. Investigation of metal–buffer interactions using isothermal titration calorimetry. *J. Therm. Anal. Calorim.* **2013**, *111*, 1829–1836. [CrossRef]
51. Nastyshyn, S.; Pop-Georgievski, O.; Stetsyshyn, Y.; Budkowski, A.; Raczkowska, J.; Hruby, M.; Lobaz, V. Protein corona of $SiO_2$ nanoparticles with grafted thermoresponsive copolymers: Calorimetric insights on factors affecting entropy vs. enthalpy-driven associations. *Appl. Surf. Sci.* **2022**, *601*, 154201. [CrossRef]
52. Prozeller, D.; Morsbach, S.; Landfester, K. Isothermal titration calorimetry as a complementary method for investigating nanoparticle-protein interactions. *Nanoscale* **2019**, *11*, 19265–19273. [CrossRef]